

Final results of the MEG experiment

TOSHINORI MORI on behalf of MEG COLLABORATION

ICEPP, The University of Tokyo - Bunkyo-ku, Tokyo 113-0033, Japan

received 26 July 2016

Summary. — Transitions of charged leptons from one generation to another are basically prohibited in the Standard Model because of the mysteriously tiny neutrino masses, although such flavor-violating transitions have long been observed for quarks and neutrinos. Supersymmetric Grand Unified Theories (SUSY GUT), which unify quarks and leptons as well as their forces, predict that charged leptons should also make such transitions at small but experimentally observable rates. The MEG experiment was the first to have explored one of such transitions, $\mu^+ \rightarrow e^+\gamma$ decays, down to the branching ratios predicted by SUSY GUT. Here we report the final results of the MEG experiment based on the full dataset collected from 2009 to 2013 at the Paul Scherrer Institut, corresponding to a total of 7.5×10^{14} stopped muons on target. No excess for $\mu^+ \rightarrow e^+\gamma$ decays was found. Thus the most stringent upper bound was placed on the branching ratio, $\mathcal{B}(\mu^+ \rightarrow e^+\gamma) < 4.2 \times 10^{-13}$ at 90% C.L., about 30 times tighter than previous experiments, and severely constrains SUSY GUT and other well-motivated theories. We are now preparing the upgraded experiment MEG II with the aim to achieve a sensitivity of 4×10^{-14} after three years of data taking. It is expected to start late in 2017.

1. – Neutrino oscillations, GUT and $\mu^+ \rightarrow e^+\gamma$ decays

Last year's physics Nobel Prize was awarded for the discovery of neutrino oscillations. This discovery taught us two things: 1) lepton flavor is violated. Thus transitions of charged leptons such as $\mu^+ \rightarrow e^+\gamma$ should naturally occur. 2) Surprisingly the masses of neutrinos are orders of magnitude smaller than those of quarks and charged leptons.

On the one hand mysteriously small neutrino masses suppress the charged lepton transitions so much that these transitions are essentially forbidden in the Standard Model. On the other hand they seem to hint that neutrinos are Majorana and that their right-handed partners may exist in the mass range of 10^9 – 10^{12} GeV, as required by the see-saw mechanism. Then, through the evolution of the renormalization group equation (RGE) from such an ultra-high energy down to our world, the rates of the charged lepton transitions grow to an observable level, *e.g.* $\mathcal{B}(\mu \rightarrow e\gamma) \sim 10^{-12}$, even if the lepton flavor is conserved at the ultra-high energy [1].

The ultra-high mass scale suggested by the see-saw mechanism may be indicative of their connection to SUSY GUT that unify the strong and electroweak forces at $\mathcal{O}(10^{16})$ GeV. It was also shown that GUT themselves make the charged lepton transitions grow to a similar level, $\mathcal{B}(\mu \rightarrow e\gamma) \sim 10^{-12}$, through the RGE evolution [2].

Over the last five years we have seen two epoch-making developments in particle physics: discoveries of Higgs and the third neutrino oscillation, θ_{13} . The fact that the Higgs boson is rather light (~ 125 GeV) suggests that the Higgs is likely to be elementary and our theory may be safely extrapolated up to ultra-high energy where see-saw mechanism and/or GUT may be realized. And the observed large mixing angle $\theta_{13} \simeq 9^\circ$ means that even higher $\mathcal{B}(\mu \rightarrow e\gamma)$ is expected in many physics scenarios.

In addition, if some TeV-scale new physics causes the tantalizing deviation of the anomalous magnetic moment of muons, $(g_\mu - 2)$, from the Standard Model by more than 3σ [3], it should also cause $\mu^+ \rightarrow e^+\gamma$ decays at an experimentally measurable branching ratio with a reasonable assumption of flavor violation [4].

Although TeV-scale new physics has been explored so much by the LHC experiments, components of new physics that are not strongly interacting are not much constrained yet. Searches for charged lepton transitions like $\mu^+ \rightarrow e^+\gamma$ are more sensitive to those components and are thus complementary and synergetic to the LHC experiments in exploring TeV-scale new physics.

2. – The MEG experiment

A $\mu \rightarrow e\gamma$ decay is characterized by an electron and a photon emitted back-to-back with energy equal to half the muon mass (52.8 MeV) in the rest frame of the muon. Positive muons are used to avoid the formation of muonic atoms in the muon stopping target. To explore the tiny branching ratio of the range 10^{-12} – 10^{-13} , an enormous number of stopped muons ($\geq 10^7$ μ/s) must be prepared by a high-power accelerator. In such high-rate environment the leading source of the background is an accidental overlap of a Michel positron and a photon from a radiative muon decay (RMD) or annihilation of a positron in flight (AIF).

The world's most intense continuous μ^+ beam of more than 10^8 μ^+/s made available by the 2.2 mA proton cyclotron at the Paul Scherrer Institut (PSI), Switzerland, is the unique tool for such a high sensitivity $\mu^+ \rightarrow e^+\gamma$ decay search. The MEG experiment [5, 6], first proposed in 1999, started searching for $\mu^+ \rightarrow e^+\gamma$ decay at PSI in 2008.

Major challenges for the experiment are 1) a capability to manage and measure $\geq 10^7$ positrons emitted every second from muon decays, and 2) high-resolution photon measurements, especially in energy, to suppress accidental photons from RMD and AIF.

In the MEG experiment (fig. 1), a gradient magnetic field specially configured by a superconducting magnet consisting of five co-axial coils with different radii [7] enables selective measurements of positrons with a momentum close to that of signal positrons. The He-based, low material drift chamber system ensures that the total material along a signal positron trajectory amounts to only $2.0 \times 10^{-3} X_0$, thus reducing multiple scatterings, the dominant source of error in e^+ measurements, to a minimum [8]. The e^+ timing is measured by arrays of 4 cm thick plastic scintillator bars placed at a larger radius to avoid low-momentum e^+ hitting them [9].

A homogeneous calorimeter that can contain fully the shower induced by the 52.8 MeV photon and yields large, fast signals, is the key to high-resolution photon measurements. In the MEG photon detector, a volume of 900 ℓ liquid xenon (LXe) is surrounded by 846 photomultipliers that are submerged directly in the LXe and collect VUV scintillation

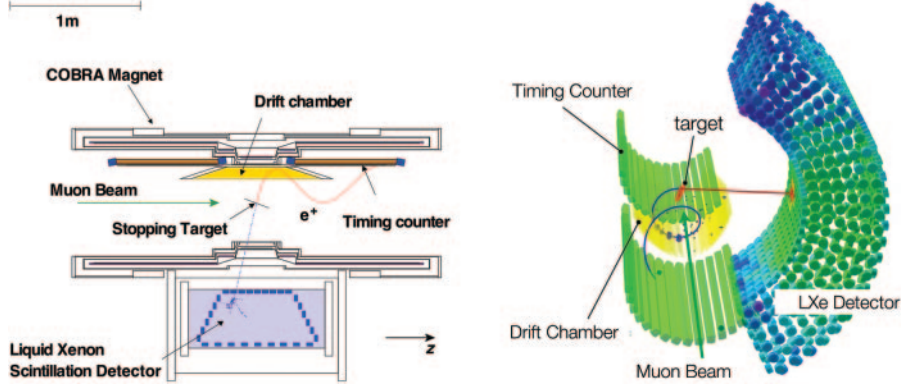


Fig. 1. – Left: a schematic view of the MEG experiment showing a simulated $\mu^+ \rightarrow e^+\gamma$ event. Right: a 3D display of an accidental background event observed by the MEG detector.

lights from the LXe [10]. It achieved resolutions of 1.6–2.3% in energy, 64 ps in timing, and 5 mm in position of photon conversion. Photons that pile up in the detector are efficiently separated using spacial and temporal distributions of waveforms from individual photomultipliers.

Experimental tools to precisely calibrate and monitor the detectors are essential ingredients for a successful $\mu^+ \rightarrow e^+\gamma$ search. A dedicated run for $\pi^-p \rightarrow \pi^0n$ with a liquid hydrogen target was carried out each year for the absolute calibration of the LXe detector using monochromatic photons of 55 MeV from back-to-back π^0 decays (fig. 2), while the stability of the calibration was monitored by the photon spectrum of RMD and AIF (fig. 3) as well as 17.6 MeV photons from $p+{}^7\text{Li} \rightarrow {}^8\text{Be}+\gamma$ in weekly calibration runs using the dedicated Cockcroft-Walton proton accelerator. The photon energy scale was confirmed to be stable within 0.2% during the whole data taking periods (fig. 4). The positron momentum was calibrated and monitored using the upper end-point of Michel

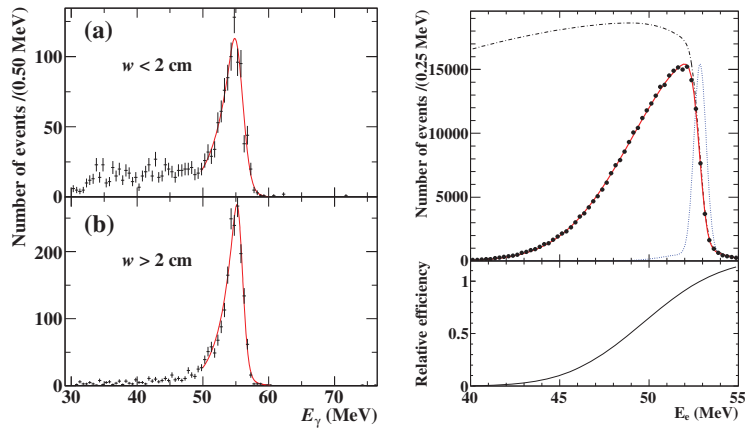


Fig. 2. – Left: energy response of the LXe detector for 55 MeV photons from $\pi^-p \rightarrow \pi^0n$. Here w is the distance from the conversion point to the photomultiplier surface. Right: the measured Michel e^+ spectrum fitted to obtain the scale and resolution of momentum measurements.

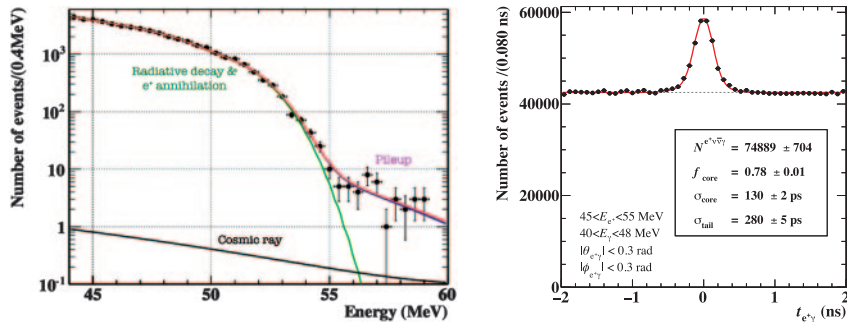


Fig. 3. – Distributions of side-band data. Left: the photon spectrum is fitted to monitor the scale and resolution of the energy measurement (fig. 4). Right: the photon-positron timing distribution showing separate components of radiative muon decays (RMD) and accidental background provides the relative timing and resolution of the timing measurement.

spectrum (fig. 2), while positrons that turned more than once within the drift chamber system were used to evaluate angular measurements by comparing measurements of individual turns. RMDs measured during the physics run were used to calibrate and monitor the timing between photons and positrons (fig. 3).

A more detailed description of the MEG detector including various calibration and monitoring tools that are not covered here is available in [11].

3. – The $\mu^+ \rightarrow e^+\gamma$ decay search

Approximately half of the data taken by the MEG experiment had been previously analyzed and published [12-14]. Here we report the results of the analysis using the whole MEG data with updated, improved calibration and analysis methods [15].

Our analysis strategy is a combination of blind and maximum likelihood analysis. A rather large region of data was blinded ($|t_{e^+\gamma}| < 1$ ns and $48 < E_\gamma < 58$ MeV) and a region for likelihood analysis was defined within the blinded region. The accidental background dominated the MEG data with the RMD background only $< 1/10$ of the accidental. The background distributions in the analysis region, therefore, were reliably evaluated from the side-band data. A fully frequentist approach was adopted for the likelihood fits with profile likelihood ratio ordering.

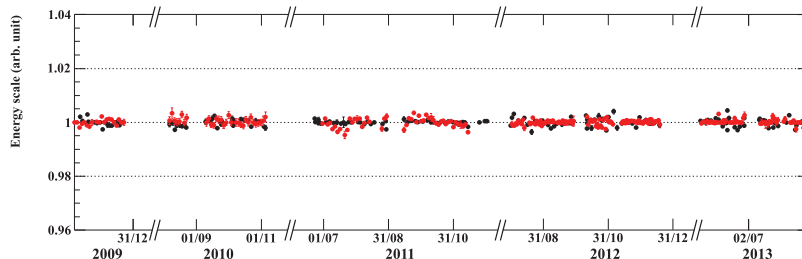


Fig. 4. – Stability of photon energy scale for the whole data taking periods. The rms spread is less than 0.2%. The red circles are the 17.6 MeV photon peak from ⁷Li and the black circles the energy scale fitted from the background spectrum (fig. 3).

TABLE I. – *Best fit branching ratios, 90% C.L. upper limits and expected sensitivities ($\times 10^{-13}$) for different datasets.*

Dataset	2009–2011	2012–2013	All
Best fit	–1.3	–5.5	–2.2
90% C.L. upper limit	6.1	7.9	4.2
Expected sensitivity	8.0	8.2	5.3

Probability density functions (PDFs) necessary for the likelihood analysis were obtained from the side-band and the calibration data taking into account correlations between observables, and different PDFs were used for each event depending on the detector conditions and the hit position in the detector. The use of the event-by-event PDFs improves the analysis sensitivity by about 20% over the constant PDFs.

To convert the number of signal events into a branching ratio, the number of muon decays effectively measured during the experiment was evaluated and cross-checked by two independent methods that count Michel decays and RMDs. The obtained single event sensitivity for the full dataset is 5.84×10^{-14} with a 3.5% uncertainty.

Improvements over the previous publication include 1) reconstruction and removal of background AIF photons that originated from inside the drift chamber system, 2) recovery of partially missing trajectories of multi-turn e^+ s ($\approx 4\%$ gain in efficiency), and 3) better understanding in photomultiplier alignment inside the LXe detector.

A non-negligible approximately paraboloidal deformation of the stopping target (a $205 \mu\text{m}$ thick layer of polyethylene and polyester) was found for the 2012–2013 runs with a maximum systematic uncertainty of 0.3–0.5 mm along the beam axis. This represents a single dominant systematic error that degraded the sensitivity by 13% on average while the total contribution of all the other systematic uncertainties is less than 1%.

The expected sensitivity of the analysis was evaluated by taking the median of the 90% C.L. branching ratio upper limits obtained for an ensemble of pseudo experiments with a null signal hypothesis and all systematic uncertainties taken into account (table I). The maximum likelihood analysis was also tested using the side-bands and the obtained upper limits were found consistent with the distribution for the pseudo experiments.

The blinded region was opened after the analysis tools were optimized and the background studies in the side-bands were completed. The event distributions inside the analysis region are shown in fig. 5. No significant correlated excess is observed within the signal contours.

A maximum likelihood analysis was performed and the number of signal events in the analysis window was evaluated and converted into branching ratios (table I). The projections of the best fitted likelihood function are shown in fig. 6(a)–(e); they are in good agreement with the data. The relative signal likelihood R_{sig} defined as $R_{\text{sig}} \equiv \log_{10}(S/(f_R R + f_A A))$ is plotted in fig. 6(f) where S , R and A are the PDFs for signal, RMD and accidental and f_R and f_A are the expected fractions of the two backgrounds. The data fit pretty well with the background distribution.

The upper limit of the confidence interval was calculated in a frequentist approach to be 4.2×10^{-13} at 90% C.L. for the whole dataset. This represents a significant improvement by a factor 30 compared with the previous experiment [16] (fig. 7).

In fig. 7 two other charged lepton transitions involving muons, $\mu^- N \rightarrow e^- N$ and $\mu^+ \rightarrow$

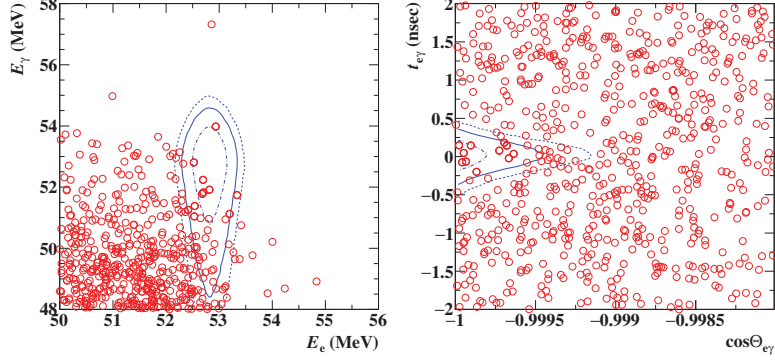


Fig. 5. – Event distributions for the full dataset. Selection cuts with 90% efficiency each for $\cos \Theta_{e+\gamma}$ and $t_{e+\gamma}$ in the left figure, and 74% for E_γ and 90% for E_{e^+} in the right figure are applied ($\cos \Theta_{e+\gamma} < -0.99963$; $|t_{e+\gamma}| < 0.24$ ns; $51.0 < E_\gamma < 55.5$ MeV; $52.4 < E_{e^+} < 55.0$ MeV). The signal PDF contours corresponding to 1σ , 1.64σ and 2σ are also shown.

$3e$, are also plotted for comparison. Here their experimental upper bounds are converted into equivalent $\mu^+ \rightarrow e^+\gamma$ branching ratios, assuming that they proceed predominantly with electromagnetic transitions similar to $\mu^+ \rightarrow e^+\gamma$ and therefore their rates are simply related to $\mu^+ \rightarrow e^+\gamma$ branching ratios in the following way: $\mathcal{B}(\mu^+ \rightarrow 3e) \simeq 1/170 \times \mathcal{B}(\mu \rightarrow e\gamma)$ and $R(\mu^- \text{Al} \rightarrow e^- \text{Al}) \simeq 1/390 \times \mathcal{B}(\mu \rightarrow e\gamma)$ [17]. These relations indicate relative physics sensitivity of these processes in supersymmetric models where electromagnetic transitions normally dominate.

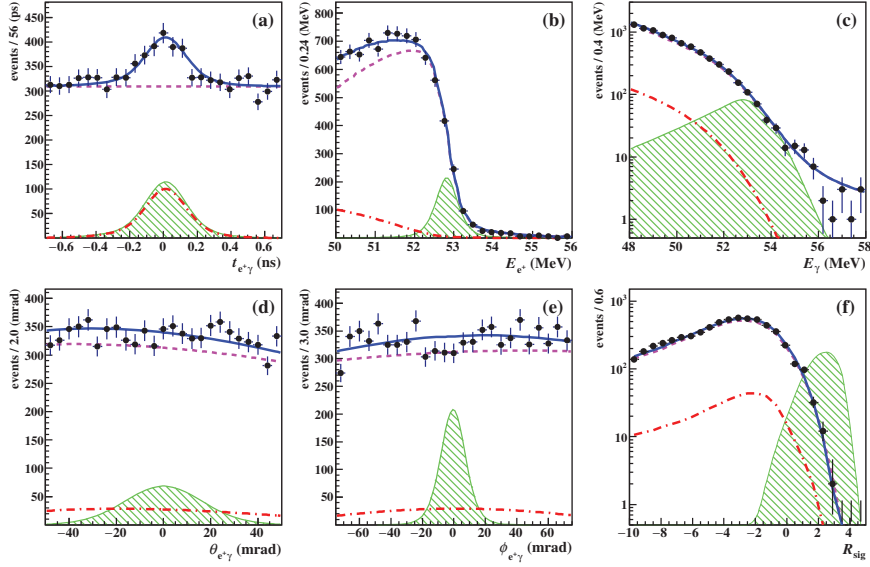


Fig. 6. – The distributions of the best fitted likelihood function and R_{sig} (see text) together with those of the full MEG data. The individual components for accidental background (dash lines) and radiative muon decays (dot-dash) are also shown. The green hatched histograms are the signal PDFs corresponding to 100 times magnified upper limit on signal events.

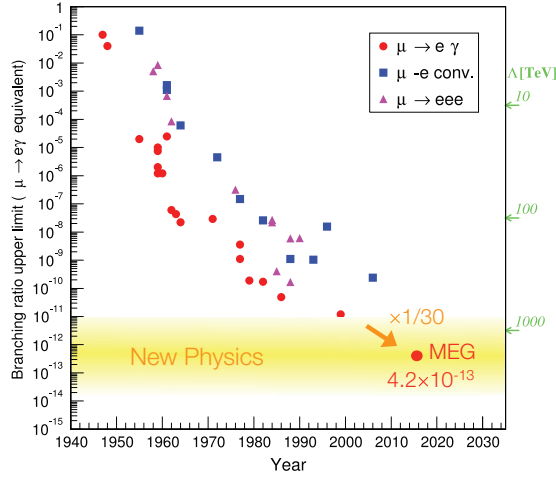


Fig. 7. – Experimental upper limits (90% C.L.) on the three flavor-violating muon processes as a function of the year. The bounds for $\mu^+ \rightarrow 3e$ and $\mu^- N \rightarrow e^- N$ are converted into equivalent $\mu^+ \rightarrow e^+ \gamma$ bounds (see text). The result presented in this report is highlighted.

4. – The MEG II experiment

In 2013 our proposal for upgrading the MEG detectors to improve the experimental sensitivity by an order of magnitude [18] was approved by the PSI research committee.

The basic idea is to achieve the highest possible sensitivity by making maximum use of the available muon intensity at PSI with improved detectors, since we had to reduce the intensity for a stable operation of the detector and to keep background at a manageable level in the MEG experiment. Other main improvements of MEG II include: 1) larger detector acceptance by more than a factor 2 by diminishing materials between the new single-volume drift chamber and the timing counter; 2) improved resolutions for photons with more uniform collection of scintillation light by replacing the phototubes with new VUV-sensitive $12 \times 12 \text{ mm}^2$ SiPMs; 3) improved resolutions for e^+ with arrays of thin scintillator tiles to achieve a 30 ps resolution with ≈ 9 hit tiles per e^+ and better position resolution and more hits per track of the new drift chamber with small stereo cells; and 4) further background suppression with a pair of counters to actively tag RMD photons by detecting the associated low-momentum e^+ 's. A thinner but more solid target ($\approx 140 \mu\text{m}$ thick) with a beam-monitoring capability is also being studied to control target-related systematic uncertainties.

Upgraded detectors are currently being constructed. A quarter of the timing counter was installed and tested under the actual MEG II beam condition using a newly developed trigger and DAQ electronics system. A full engineering run is scheduled in 2017 and may evolve into physics run if things get ready. A few months of data taking will be sufficient to exceed the MEG sensitivity. To reach the final sensitivity goal of 4×10^{-14} will require 3 years of data taking.

With other muon experiments joining the race soon, MEG II will continue to lead charged lepton flavor violation searches in the coming years.

* * *

We are grateful for the support and cooperation provided by PSI as the host laboratory and to the technical and engineering staff of the collaborating institutes. This work is

supported by MEXT KAKENHI 22000004 and 26000004 in Japan, INFN in Italy, SNF Grant 200021_137738 in Switzerland, DOE DEFG02-91ER40679 in USA, and RFBR-14-22-03071 in Russia.

REFERENCES

- [1] HISANO J. and NOMURA D., *Phys. Rev. D*, **59** (1999) 116005.
- [2] BARBIERI R. and HALL L. J., *Phys. Lett. B*, **338** (1994) 212; BARBIERI R., HALL L. J. and STRUMIA A., *Nucl. Phys. B*, **445** (1995) 219.
- [3] MUON G-2 COLLABORATION (BENNETT G. W. *et al.*), *Phys. Rev. D*, **73** (2006) 072003.
- [4] ISIDORI G., MESCIA F., PARADISI P. and TEMES D., *Phys. Rev. D*, **75** (2007) 115019.
- [5] MORI T. *et al.*, *Research Proposal to Paul Scherrer Institut* (PSI Proposal R-99-05) (1999) https://meg.web.psi.ch/docs/prop_psi/proposal.pdf.
- [6] MEG COLLABORATION (BALDINI A. M. *et al.*), *Research Proposal to INFN* (2002) https://meg.web.psi.ch/docs/prop_infn/nproposal.pdf.
- [7] OOTANI W. *et al.*, *IEEE Trans. Appl. Supercond.*, **14** (2004) 568.
- [8] HILDEBRANDT M., *Nucl. Instrum. Methods A*, **623** (2010) 111.
- [9] DE GERONE M. *et al.*, *IEEE Trans. Nucl. Sci.*, **59** (2012) 379.
- [10] SAWADA R., *Nucl. Instrum. Methods A*, **623** (2010) 258.
- [11] MEG COLLABORATION (ADAM J. *et al.*), *Eur. Phys. J. C*, **73** (2013) 2365.
- [12] MEG COLLABORATION (ADAM J. *et al.*), *Nucl. Phys. B*, **834** (2010) 1.
- [13] MEG COLLABORATION (ADAM J. *et al.*), *Phys. Rev. Lett.*, **107** (2011) 171801.
- [14] MEG COLLABORATION (ADAM J. *et al.*), *Phys. Rev. Lett.*, **110** (2013) 201801.
- [15] MEG COLLABORATION (BALDINI A. M. *et al.*), *Eur. Phys. J. C*, **76** (2016) 434.
- [16] MEGA COLLABORATION (BROOKS M. L. *et al.*), *Phys. Rev. Lett.*, **83** (1999) 1521.
- [17] MORI T. and OOTANI W., *Prog. Part. Nucl. Phys.*, **79** (2014) 57.
- [18] MEG II COLLABORATION (BALDINI A. M. *et al.*), *MEG Upgrade Proposal* (PSI Proposal R-99-05.2) (2013), [arXiv:1301.7225](https://arxiv.org/abs/1301.7225).